Missing final states and the spectral endpoint in exciton model calculations

C. Kalbach

Physics Department, Duke University, Durham, North Carolina 27708-0305, USA

Recent studies of (n, xp) spectra at incident energies of 28 to 63 MeV have emphasized a previously noted trend that exciton model calculations do not extend to high enough emission energies in some (p, xn) and (n, xp) reactions. Improved agreement between experiment and calculation is achieved by including in the residual nucleus state density those configurations that can be populated but were not being counted because the Fermi level moves down during particle emission. This necessitates minor adjustments in other model parameters. The situation is generalized to reactions with complex particle channels, and significant effects are seen in the calculations for a few reactions on light targets, though the average level of agreement with experiment is unchanged from earlier work.

I. INTRODUCTION

It is clear that statistical models of nuclear reactions are going to have difficulty describing particle emission cross sections near the endpoint of an energy spectrum, where the excitation energy in the residual nucleus is low and statistical state density models are least applicable. Even considering this inherent difficulty, however, a troubling feature of a couple of earlier studies [1,2] is the extent to which the exciton model preequilibrium reaction calculations fail to extend to the highest emission energies seen in measured inclusive energy spectra for (n, xp) reactions on odd-Z targets up to around mass 70. A review of earlier results on (p, xn) reactions shows a similar problem for a few odd-N targets. Careful examination of the states in the composite and residual nuclei points to an explanation and a solution: there are configurations included in the composite nucleus state densities that, after undergoing particle emission, are not counted in the residual state density because the Fermi level has shifted down. This article first presents a method for including those states in the residual nucleus state densities, then considers the changes this requires to the existing global input parameters, and finally shows the effects produced on agreement with measured inclusive energy spectra from the literature. No new model parameters are introduced.

II. THE MISSING STATES

To understand the nature of the residual states that are not being counted, it is helpful to recall the distinction between active and passive particles and holes. Here, the term *particles* denotes filled single particle states above the Fermi level and *holes* denotes empty states below it. Because the Fermi level lies halfway between the last filled and first vacant single-particle states for a nucleus in its ground state, the number of particles and holes must always be equal, but not all of them will represent degrees of freedom. Those that are constrained by the reaction mechanism to lie adjacent to the Fermi level are called passive, whereas the remainder are termed active and represent degrees of freedom of the system. Both contribute to the energy requirement for the configuration imposed by the

Pauli exclusion principle, but only the degrees of freedom are counted in designating the configuration.

In the exciton model, as in most other preequilibrium models, the states of the nucleus are classified by the number of particle and hole degrees of freedom (or excitons) they contain. In a two-component model, where a distinction is made between proton and neutron degrees of freedom, a state is then specified by its excitation energy and the four integer variables p_π, h_π, p_ν, and h_ν, which represent, respectively, the numbers of proton particle, proton hole, neutron particle and neutron hole degrees of freedom.

To return to the problem at hand, the difficulty in reproducing the experimental spectral endpoints comes when $h_\pi > p_\pi$ in the residual nucleus after emission of a particle with $Z \geqslant 1$ or in the analogous situation for neutrons. This is most easily seen in the first stage of an (n, p) or (p, n) reaction. For direct proton emission to occur in an (n, p) reaction, the incident neutron must excite a proton particle-hole pair in the first interaction. This forms a $(p_\pi, h_\pi, p_\nu, h_\nu) = (1, 1, 1, 0)$ state, which can emit either a proton or a neutron. Neutron emission in this case produces states with $(p_\pi, h_\pi, p_\nu, h_\nu) = (1, 1, 0, 0)$. Here $p_\pi = h_\pi$ and $p_\nu = h_\nu$, and all of the residual states are correctly counted. Proton emission, however, leads to a $(p_\pi, h_\pi, p_\nu, h_\nu) = (0, 1, 1, 0)$ configuration, which has a passive proton particle and a passive neutron hole in addition to the two degrees of freedom. The proton single-particle states in the composite and residual nuclei are shown schematically in Fig. 1, because these are where the problem is seen. The neutron part of the configuration is unchanged during proton emission.

Here, the usual exciton model state density in the composite nucleus includes the three cases shown in Fig. 1: (1) a general one-proton-particle, one-proton-hole configuration; (2) the configuration in which the proton *particle* degree of freedom occupies, by chance, its lowest-lying single particle state, the one adjacent to the Fermi level; and (3) the configuration in which the proton *hole* degree of freedom is adjacent to the Fermi level. Once proton emission occurs, the proton Fermi level moves down one single-particle spacing, producing the residual states shown on the right side of the figure. [Emission (2) would normally not be energetically possible because of
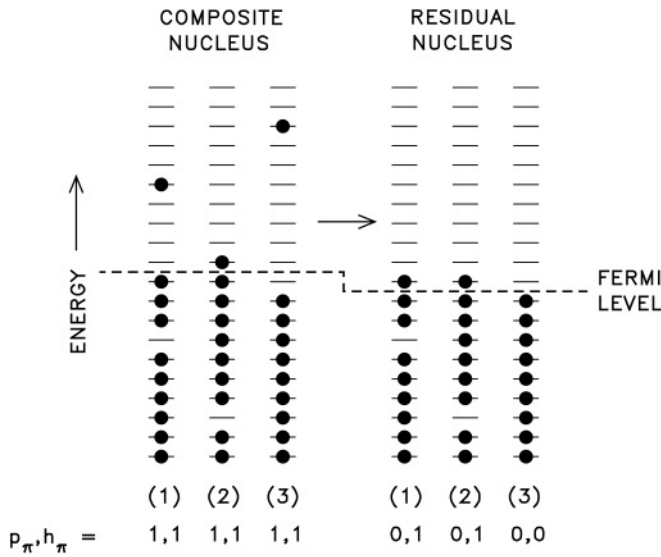
FIG. 1. Schematic diagram of the proton single-particle states for the composite and residual nuclei following the initial target-projectile interaction in an (n, p) reaction. (The neutron single-particle states are not shown.) The composite nucleus state labeled (1) shows the general case; those labeled (2) and (3) are special cases in which the proton particle or proton hole degree of freedom occupies its lowest excitation energy single-particle state. The corresponding numbers for the residual nucleus show the same states after proton emission has occurred and the Fermi level has moved down. Each configuration is labeled by the number of proton particle and hole degrees of freedom it contains. Residual configurations (1) and (2) also have passive proton particles.

the binding energy requirement of the emitted proton.] The residual states typically have a proton-hole degree of freedom and a passive proton particle. However, those states corresponding to case (3), where the proton hole in the composite nucleus occupies, by chance, the single particle state adjacent to the Fermi level, no longer have a proton hole in the residual nucleus. They have $p_\pi = h_\pi = 0$, and would not be counted. Therefore the $(p_\pi, h_\pi, p_\nu, h_\nu) = (0, 0, 1, 0)$ state density must be explicitly added to the usual $(0, 1, 1, 0)$ residual nucleus state density. This addition is most important when the residual states have proton pairing and/or shell corrections that involve a significant minimum energy requirement. The added state density will not have that correction, because there are no proton degrees of freedom, and it will, therefore, extend to lower residual excitation energies (higher proton emission energies) in the spectrum. This is most noticeable for light targets, for which the pairing energies are larger and the state densities increase less rapidly with the number of degrees of freedom. They are also larger at lower incident energies, where the minimum energy requirements from pairing and shell corrections represent a larger fraction of the available energy.

This argument has its full validity only in two-component formulations of the exciton model that include fully configuration-specific pairing and shell corrections in the state densities. Here separate pairing energies are evaluated for neutrons and protons, with the neutron pairing correction applied only when there are neutron degrees of freedom, and

the proton pairing correction applied only if there are proton degrees of freedom. Likewise, the shell corrections depend in detail on the number of degrees of freedom of each type [3]. In exciton model formulations where shell corrections are not made and where the pairing correction does not depend independently on the numbers of proton and neutron degrees of freedom, the effect of adding the extra residual states would be much smaller, and it would likely not be possible to reproduce the measured energy spectral endpoints.

Now let us consider the general case. When a light particle of type b is emitted from the composite nucleus, the proton Fermi level will move down by Z_b single-particle states and the neutron Fermi level by N_b states, where Z_b and N_b are the proton and neutron numbers of the emitted particle. Thus there will be Z_b proton single-particle states and N_b neutron single-particle states that were accessible to holes in the emitting nucleus but are accessible to particles in the residual nucleus. Normally, the number of hole degrees of freedom in a configuration does not change during particle emission, but a composite nucleus configuration in which a hole degree of freedom happens, by chance, to occupy one of these single-particle states, would actually lead to a residual nucleus state with one less hole degree of freedom. This would imply that we should add to the residual nucleus state density those configurations that have up to Z_b fewer proton hole degrees of freedom and up to N_b fewer neutron hole degrees of freedom. The usual state density in the residual nucleus, $\omega(p_\pi, h_\pi, p_\nu, h_\nu, U)$, would then be replaced by an effective state density,

$$\omega_{\text{eff}}(p_\pi, h_\pi, p_\nu, h_\nu, U) = \sum_{i=h_\pi-Z_b}^{h_\pi} \sum_{j=h_\nu-N_b}^{h_\nu} \omega(p_\pi, i, p_\nu, j, U),$$
(1)

where U is the excitation energy in the residual nucleus. However, the effect of passive holes in the emitting nucleus still needs to be considered.

When a light projectile fuses with a target nucleus, the states in the composite system will typically have $p_\pi - h_\pi = Z_a$ and $p_\nu - h_\nu = N_a$, where Z_a and N_a are the proton and neutron numbers of the projectile. Thus there will be Z_a passive proton holes and N_a passive neutron holes, which were formed when the Fermi level moved up as the target and projectile fused. Each passive hole occupies one of the single-particle states just below the Fermi level, so that these states are not accessible to the active holes. This means that the corresponding auxiliary configurations are not populated in the residual nucleus. The auxiliary configurations will thus be limited to having up to $Z_b - Z_a$ fewer proton degrees of freedom than the main configurations and similarly for neutrons. If $Z_a \geqslant Z_b$ or $N_a \geqslant N_b$ there will be no auxiliary configurations for that particle type. This is the case for inelastic scattering. The lower limit in the sum over i now becomes $h_\pi - \max(Z_b - Z_a, 0)$, with an analogous expression for j. Recalling that $Z_b - Z_a$ is the number of passive proton particles in the residual nucleus (or minus the number of passive proton holes if $Z_a > Z_b$) and is also equal to $h_\pi - p_\pi$, the effective residual nucleus state density, $\omega_{\text{eff}}(p_\pi, h_\pi, p_\nu, h_\nu, U)$, becomes the following:

$$\omega_{\text{eff}}(p_\pi, h_\pi, p_\nu, h_\nu, U) = \sum_{i=i_{\min}}^{h_\pi} \sum_{j=j_{\min}}^{h_\nu} \omega(p_\pi, i, p_\nu, j, U), \quad (2)$$
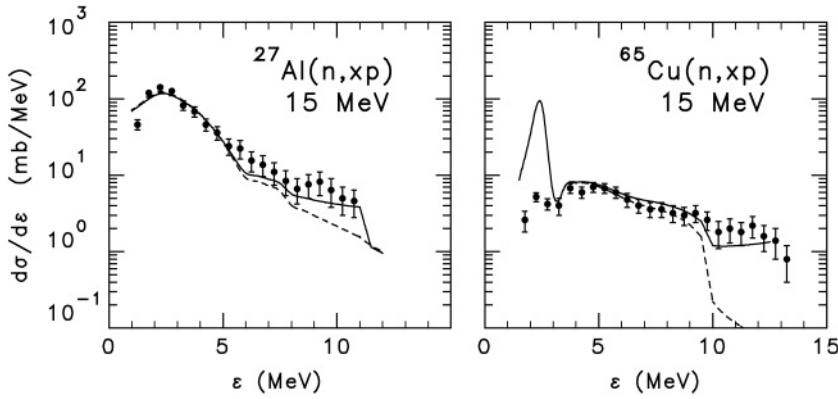
FIG. 2. Effects of including the extra residual states in the calculations for (n, xp) spectra for two sample reactions. The solid and dashed curves show the calculated results with and without, respectively, the extra states included and are plotted vs. channel energy. The points show the data from Refs. [8,9] and are given in terms of the laboratory energy of the emitted particle.

where $i_{\min} = \min(p_\pi, h_\pi)$ and $j_{\min} = \min(p_\nu, h_\nu)$. This reverts to the normal state density when $p_\pi \geqslant h_\pi$ and $p_\nu \geqslant h_\nu$. It should be noted, however, that the expressions for $i_{\min}$ and $j_{\min}$ are only valid for particle emission from the initial composite nucleus. The missing states have not been included for subsequent, or secondary, particle emission, for which the lower limits take on a more complicated form.

III. INCLUDING THE MISSING STATES

The preequilibrium reaction computer code PRECO-2000 [4] has previously been modified with regard to surface localization of the initial interaction of incident neutrons [5] and with regard to the complex particle channels [2]. It is this modified version with the default global input parameters that has been used in the present work. Pairing and shell structure effects are included, and isospin is assumed to be conserved as a quantum number if the composite nucleus excitation energy is less than four times the symmetry energy [6]. The residual nucleus state densities used in calculating the exciton model particle emission rates for the various composite nucleus states have now been modified to use Eq. (2) in place of the usual $\omega(p_\pi, h_\pi, p_\nu, h_\nu, U)$. Calculations were run with the modified code and the results were compared with many (though not all) of the angle integrated spectra in the database from Refs. [2,5,7]. In all, 250 spectra were compared with experiment as well as with the results of earlier calculations. These include spectra with both nucleon and light complex particle channels. In this section, the emphasis is on the nucleon channels, whereas the next section discusses broader comparisons with the data.

A. Improvement in spectral endpoints for (N, xN) reactions

For (N, xN) reactions, where N is a nucleon, the effect of the added residual configurations is to increase the preequilibrium yield in the exchange channels, though the increase is most significant at the highest emission energies. In inelastic scattering, however, the residual states always have $p_\pi = h_\pi$ and $p_\nu = h_\nu$, so no new residual configurations are being included and the calculated spectra are almost unchanged. For this reason, more exchange than inelastic spectra were studied in this work. The effect observed is largest when the extra residual configurations have a significantly lower minimum energy requirement than the main configurations. In most cases, agreement with experiment

at the highest emission energies is either significantly improved or virtually unchanged, and the calculated preequilibrium spectral endpoints are quite reasonable. Note that these changes introduce no new free parameters. Two examples are shown in Fig. 2.

For the ^{27}Al(n, xp) reaction at 15 MeV [8], the change is largely the result of pairing. This tends to be important for (n, xp) on odd-Z targets and (p, xn) on odd-N targets at lower mass numbers where the pairing energies are relatively large. Previously, the calculated ^{27}Al(n, xp) cross section at emission energies of 8–12 MeV was all due to the tail of the evaporation component. Now, the proton pairing energy requirement of 2.2 MeV disappears for the added residual configurations from first-stage preequilibrium emission, because these states have no proton degrees of freedom. Thus the high-energy part of the calculated spectrum is filled in.

A large energy requirement because of a shell closure can also cause a significant effect to occur. In Fig. 2, this is seen in the ^{65}Cu(n, xp) reaction at 15 MeV [9], where the ^{65}Ni residual nucleus has a closed shell at $Z = 28$. For first stage (or direct) preequilibrium emission, the proton hole degree of freedom in the residual nucleus causes the shell gap to enter into the minimum energy requirement from the Pauli exclusion principle. This hole degree of freedom is absent in the added configurations, thus lowering the configuration energy requirement by about 1.5 MeV. This is reinforced by the proton pairing energy, also of 1.5 MeV. The improvement with the present calculation is dramatic.

The effects in the exchange channels typically diminish as the target mass and the excitation energy increase. There are only a few exchange spectra for which inclusion of the additional residual configurations worsens agreement between calculation and experiment at high emission energies. These are ^{93}Nb(n, xp) at 14.1 and 15 MeV [10–13], ^{115}In(n, xp) at 14.1 MeV [12], and those ^{A}Zr and ^{A}Mo(p, xn) reactions at 18 and 25 MeV [14] where the residual nucleus has a neutron number slightly above the $N = 50$ shell closure. The ^{93}Nb data have been measured several times and are firmly established. However, several other reactions in this region have been notoriously difficult to explain; especially the ^{93}Nb$(n, x\alpha)$ reaction, which has always been significantly overestimated. The ^{115}In(n, xp) reaction is a very weak channel and thus difficult both to measure and to calculate. The zirconium and molybdenum isotopes are discussed in Sec. III C, below.

But again, in general the results are either improved or unchanged in the region around the spectral endpoint. Comparisons with experiment are shown in Sec. IV.

B. Model parameter adjustments

Although the inclusion of the missing residual states in the calculations improves agreement in spectral endpoint for some reactions that were previously difficult to explain, it is clear that the added strength is not confined to the highest emission energies. The additional cross section in the (N, N) exchange channels is not large, but for (p, xn) reactions it is enough, on average, to disturb slightly the balance between inelastic and exchange processes. To restore this balance, it was necessary to adjust the normalizations of the effective mean square matrix elements for the residual interactions leading to energy equilibration in the composite nucleus.

The mean square matrix elements in PRECO are given by the following:

$$M_{ij}^2 = K_{ij} A_a A^{-3} (20.9 + E/3A_a)^{-3},$$

where the A_a dependence was introduced in Ref. [2]. Here the subscripts i and j indicate the kinds of nucleons (neutrons or protons) involved in the interaction. The empirical normalization factors, K_{ij}, are $K_{pp} = 5.7 \times 10^6$ MeV^5 and $K_{pp} : K_{pn} : K_{nn} = 5.7 : 3.4 : 3.4$. It should be mentioned that although the general magnitude of the M^2 values can be understood in that they are significantly smaller than the full two-body matrix elements extracted from particle-particle and particle-hole multiplets of states outside a closed-shell configuration [15], the specific values of the three normalization constants are strictly empirical and were determined so as to reproduce the observed relative yields in the four (N, N) channels. They also depends on other details of the calculations. Thus there is no obvious physical explanation for their values and no reason not to make changes. One can speculate that K_{pp} is larger than the others because of the effect of the Coulomb interaction, but that is only speculation based on the fact that the Coulomb interaction is the most obvious difference between p-p interactions on the one hand and p-n or n-n interactions on the other. [Indeed, as discussed in Ref. [7], reproducing the relative yields in the four (N, N) channels is one of the major challenges facing any preequilibrium model, and without some parameter adjustment, at least one of the channels tends to be over- or underestimated. Even the recent and highly impressive work of Koning and Duijvestijn [16], which avoids the present parameter adjustment by using transition rates derived from or guided by the imaginary optical model potentials, tends, on average, to somewhat overpredict the (p, xn) yield at incident energies from 14 to 90 MeV relative to the other three channels. At still higher energies, higher than those considered in this work, the problem seems to disappear. Clearly there are elements of physics here that are not yet fully understood.]

Because no obvious difficulty was observed here in the neutron induced reactions, the condition that $K_{pn} = K_{nn}$ is retained, but the difference between these and K_{pp} is increased. The new empirical values are $K_{pp} = 7.5 \times 10^6$ MeV^5 and $K_{pp} : K_{pn} : K_{nn} = 7.5 : 3.0 : 3.0$. Although this looks like a large change, the effect on the calculated spectra is small and is concentrated, again, mainly in the (p, xn) spectra. The decrease in their intensity ranges from a few percentages to as much as 10% at the lower bombarding energies and up to 20% for the ^{27}Al(p, xn) reaction at 90 MeV. In general, agreement in intensity is now comparable to what was previously obtained or is somewhat improved.

Why is the inelastic channel not more affected by the matrix element adjustment? Two reasons are apparent from looking at the initial particle-hole pair creation, following which most of the preequilibrium emission occurs. First, in a proton-induced reaction, the inelastic channel can be populated following excitation of either a proton or a neutron particle-hole pair, so both K_{pp} and K_{pn} are involved. In the exchange channel, only K_{pn} enters. Taking into account all of the distinguishability factors in the pair creation rates [7], the relative numbers of excited protons and neutrons in the composite nucleus is, to first order: $(K_{pp} + K_{pn}) : K_{pn}$. Thus the inelastic yield is roughly independent of the balance between K_{pp} and K_{pn}, whereas the exchange yield has such a dependence. Second, the inelastic channel often carries more of the preequilibrium cross section, so that shifting a given amount of strength from the exchange to the inelastic channel will make a larger percentage change in the former.

Why do proton-induced reactions show a need to adjust the balance between the matrix element normalizations, whereas neutron induced reactions do not? This is more difficult to answer, but several factors may be noted. First, the data are sparser for incident neutrons and the balance is more difficult to determine. In particular, there are relatively few reaction systems for which both channels have been measured, and many of these are at incident energies of 14 to 15 MeV, where the evaporation component plays a large role, especially for the lighter targets. In addition, many of the (n, xp) spectra on the lighter targets were slightly underpredicted prior to this work so that the added cross section has a beneficial effect over the full preequilibrium spectrum, not just near the endpoint. The initial balance between K_{nn} and $K_{np} = K_{pn}$ was set [1] based largely on the low-energy data, whereas many more exchange spectra have since become available, so perhaps the starting balance was not optimal without the added residual configurations introduced in this work. Finally, it is also possible that additional adjustments will be needed as new data are published.

C. The washout of shell-structure effects

There is a specialized subset of the database that shows another and quite minor difficulty when the missing residual configurations are included. When a (p, xn) residual nucleus has a neutron number slightly above a neutron shell closure, or an (n, xp) residual has a proton number slightly above a proton shell closure, the emission spectrum can show a steplike structure at the higher emission energies. This structure is most pronounced in the data when the residual nucleus is one or two mass units above the shell closure and then gradually disappears in moving away from the shell closure. Such behavior is seen clearly for the $N = 50$ shell closure in the $^{92-94}$Zr(p, xn), $^{94-100}$Mo(p, xn) reactions at 18 and 25 MeV [14] mentioned above in Sec. III A. Other shell closures are
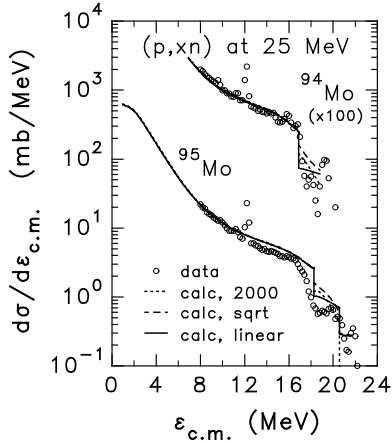
FIG. 3. Effects of modifying the rapidity with which shell effects are assumed to disappear in moving away from a closed-shell configuration. The active shell closure in these examples is at $N = 50$. The data are from Ref. [14] and are shown as the open points, whereas the three calculations correspond to the previous results (dotted curve), the corresponding results with the added residual configurations included (dashed curve), and the final results with the slower disappearance of shell effects (solid curve).

less instructive. In the $A = 50-60$ mass region and in the lead region, this kind of effect is often obscured because both a neutron and a proton shell closure are present, and there are no (n, xp) spectra for targets with proton numbers two to four units above the $Z = 50$ shell closure in the database.

In earlier work, the rapidity with which shell effects in the particle-hole state densities were assumed to wash out as N or Z moves away from a magic number was adjusted empirically using the $^A\text{Mo}(p, xn)$ data. A key element in this work was reproducing the height and sharpness of the step in the spectra. Now, with the inclusion of the extra residual states, Fig. 3 shows that the step is too gradual and not high enough. An additional adjustment is needed.

When shell effects are included in the state density calculations in PRECO, both the single-particle state densities and the configuration's minimum energy required by the Pauli principle are each evaluated using both the equispacing model (ESM) and the shell-shifted equispacing model (S^2-ESM) single-particle states, and a weighted average is taken. Initially [3], the shell effects were assumed to wash out over a range of N or Z that was given by $D/2d$, where D is the width of the shell gap and d is the single-particle level spacing in the ESM. This corresponds to the degeneracy of the single-particle levels on either side of the shell gap in the S^2-ESM. The fraction of the proton shell effects remaining was thus given by

$$F_{\pi,\text{shell}} = 1 - \frac{|Z - Z_{\text{magic}}|}{D_\pi/(2d_\pi)} \tag{3}$$

for $|Z - Z_{\text{magic}}| < D_\pi/(2d_\pi)$; otherwise it is zero. Thus $F_{\pi,\text{shell}}$ is the weighting factor for the S^2-ESM value of the proton part of the Pauli energy requirement or the proton single-particle state density being calculated, and $(1 - F_{\pi,\text{shell}})$ is the weighting factor for the corresponding ESM value. Later, when a study of shell effects in the equilibrium component was made,

a more rapid washout was assumed for both preequilibrium and equilibrium calculations, but the range of Z or N over which the washout occurs was doubled so that

$$F_{\pi,\text{shell}} = 1 - \left(\frac{|Z - Z_{\text{magic}}|}{D_\pi/d_\pi}\right)^{1/2}. \tag{4}$$

Now with the inclusion of the extra configurations, a return to the linear washout of Eq. (3) for the preequilibrium phase of the reaction is adopted, though still with the doubled range of Eq. (4) so that

$$F_{\pi,\text{shell}}^{\text{preeq}} = 1 - \frac{|Z - Z_{\text{magic}}|}{D_\pi/d_\pi}. \tag{5}$$

Equation (4) is retained for the equilibrium phase of the reaction.

At first sight, it might seem that this introduces an inconsistency in the calculations. However, the shell corrections in the two phases of the reaction are calculated rather differently, even though both use the S^2-ESM set of single-particle states. In the preequilibrium calculations, both in the exciton model and in the nucleon transfer model, the energy requirements of the Pauli principle as well as the average effective single-particle state densities for the four types of excitons (proton particles, proton holes, neutron particles, and neutron holes) are all calculated for the N and Z of the nucleus under consideration. Thus the distance from the shell closure is already taken into account, but the gradual disappearance of the shell structure as this distance increases is not taken into account. For the equilibrium calculations, however, it was necessary to calculate the shell-energy correction and the single-particle state densities for the closed-shell nucleus and to rely on the averaging with the ESM values to take account both of the extent to which the N or Z of the nucleus differs from the closed-shell configuration and of the washing out of the shell structure. As a result, it should not be surprising that a more rapid decrease of the weighting factor for the shell-corrected values should be needed in the equilibrium case.

The effect of going from the more rapid, square root washout of Eq. (4) to the more gradual, linear washout of Eq. (5) in the preequilibrium calculations is shown for the $^{94,95}\text{Mo}(p, xn)$ reactions at 25 MeV in Fig. 3. The difference is confined largely to the very highest emission energies. In the case of ^{95}Mo, there are now two shoulders or steps in the calculated curve. The lower emission energy one is because of the shell structure in the neutron single-particle states, whereas the higher energy one is because of the neutron pairing energy requirement in the residual nucleus. In earlier calculations, the spectrum simply cut off above 20.6 MeV because of the pairing energy, but now the added configurations introduced in this work can contribute above that point. Again, the data support the appropriateness of adding these configurations.

IV. COMPARISONS WITH EXPERIMENT

Having made these adjustments, it is worth comparing the results of the modified calculations with a broader sample of spectra from the database, including those with complex particles in the entrance and/or exit channel.
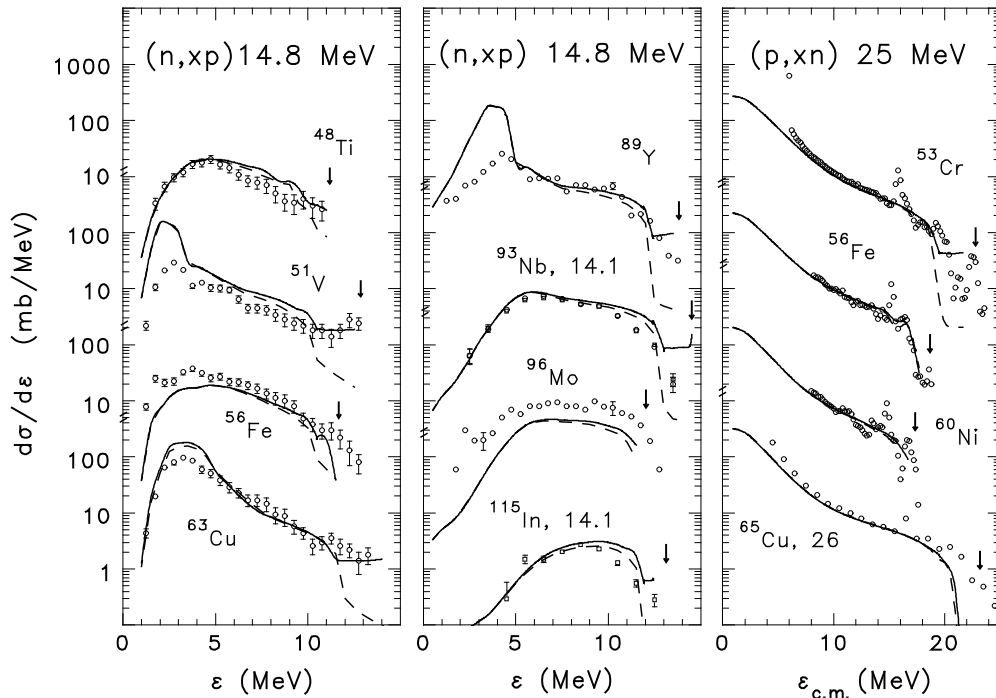
FIG. 4. Comparison between calculation and experiment for nucleon-induced exchange reactions at 15 and 25 MeV. The points show the data, taken from Refs. [8–10,12–14,17,18]; the solid curves show the present results; and the dashed curves show the earlier results, without the added residual nucleus states and prior to the parameter adjustments described in the text. The vertical arrows show the position of transitions to the ground state of the residual nucleus. For ^{63}Cu, this energy is off scale at 15.3 MeV.

A. Nucleon channels

The combined effect of adding the previously missing residual configuration and the model parameter adjustments are shown for (N, xN) reactions in Figs. 4–6. Figure 4 gives results at 14 and 25 MeV, where the data are from Refs. [8–10,12–14,17,18]. It shows the two problem spectra mentioned earlier—^{93}Nb(n, xp) and ^{115}In(n, xp)—as well as

a number of spectra for which the results are either improved or nearly unchanged relative to the previous formulation of the model.

Figures 5 and 6 are for neutron- and proton-induced reactions, respectively, at higher incident energies and include the complex particle emission spectra discussed below. The changes in the nucleon spectra are typically smaller than
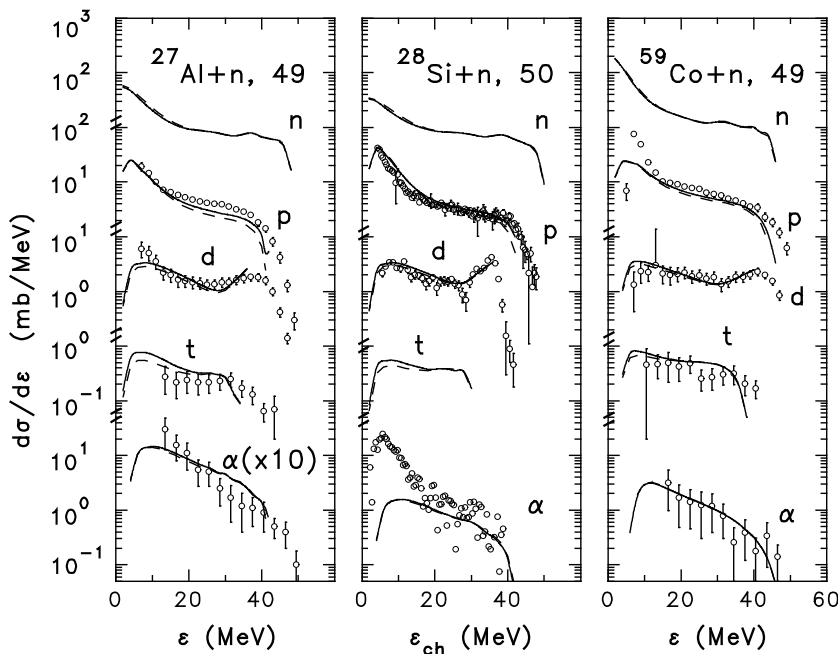
FIG. 5. Comparison between calculation and experiment for neutron-induced reactions at 49 to 50 MeV. The labels next to the curves indicate the nature of the emitted particle. The points and curves have the same significance as in Fig. 4. The data are taken from Refs. [19–21]. There are no measured neutron spectra, and the ^{28}Si(n, t) spectrum was, likewise, not reported.
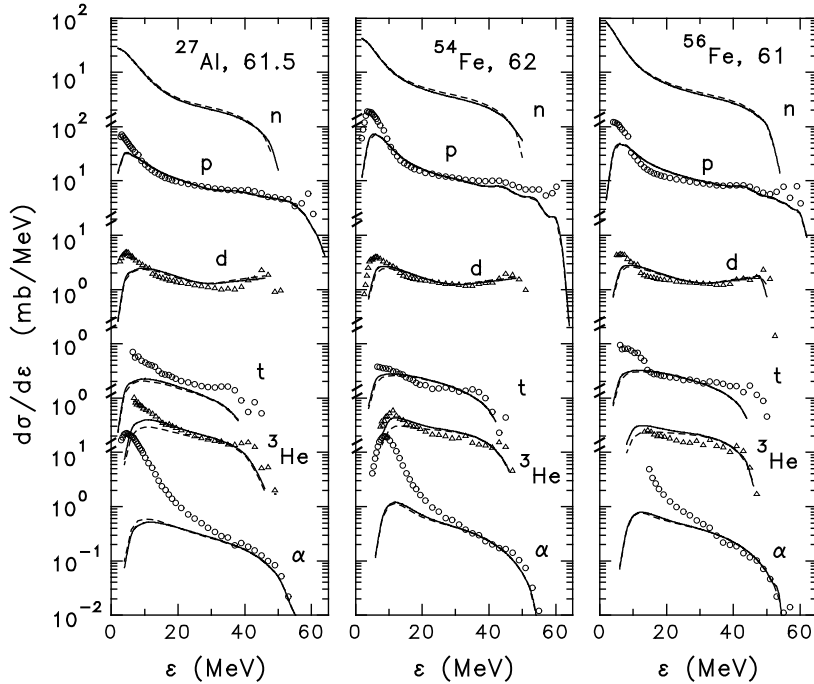
FIG. 6. Comparison between calculation and experiment for proton-induced reactions at 61 to 62 MeV. The labels next to the curves indicate the nature of the emitted particle. The points and curves have the same significance as in Fig. 4. The data are taken from Ref. [22]. There are no measured neutron spectra.

at lower incident energies, though the ^{27}Al(n, xp) results at 49 MeV are noticeably improved.

The results for heavier targets are virtually unchanged from previous calculations.
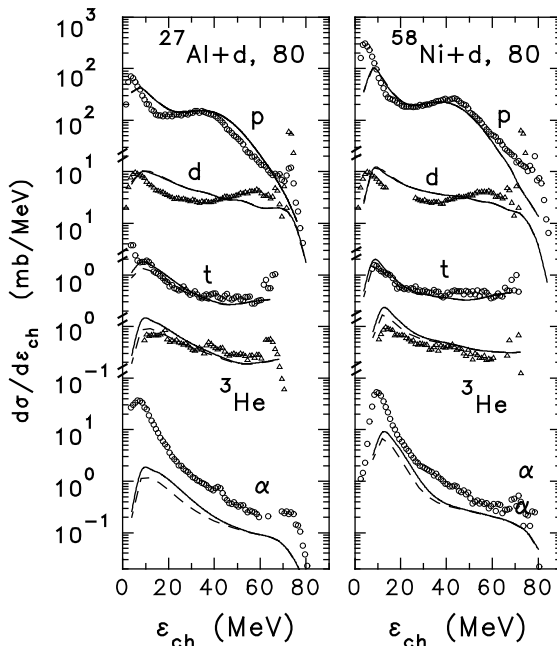
FIG. 7. Comparison between calculation and experiment for deuteron-induced reactions at 80 MeV. The labels next to the curves indicate the nature of the emitted particle. The points and curves have the same significance as in Fig. 4. The data are taken from Ref. [25]. A preliminary deuteron breakup component is included in the calculated proton spectra, but the impact of projectile breakup on the exciton model calculations is not included.

B. Complex particle channels

The discussion has so far primarily concerned reactions with nucleons in the entrance and exit channel, but a large portion of the database consists of reactions with incoming and/or outgoing complex particles. These have also been re-calculated with the added residual configurations in the exciton model and with the change in shell-structure washout, which affects both the exciton model and nucleon transfer model state densities. The additional residual nucleus configurations are needed only when $p_\pi < h_\pi$ and/or $p_\nu < h_\nu$ in the residual nucleus. This occurs for (^{3}He, t) exchange and when the emitted particle is heavier than the projectile, so this is where the largest effects are seen.

Energy spectra for the complex particle channels are largely populated by nucleon transfer processes and by direct complex particle scattering, neither of which are impacted by the added residual configurations. In addition, these mechanisms particularly dominate the end-point region of the spectrum, thus obscuring the kinds of changes the added configurations were intended to make in the (N, xN) spectra. Here, observed differences with earlier calculations are in the intensity of the exciton model component for those systems in which the added configurations are most significant, and they tend to be most visible in the lower emission energy half of the spectrum. Again, the changes are largest for the lighter targets.

Typical results for (n, xC) reactions, where C is a complex particle, are shown in Fig. 5. Agreement with experiment for some spectra is improved, whereas for a few others it is slightly worse, but overall there is no significant difference in the level of agreement between calculation and measurement. Just as the ^{27}Al(n, xp) spectra show some of the larger effects in (N, xN) reactions, so here the ^{27}Al(n, xd) and (n, xt) reactions also show the most noticeable effect. In each case, $Z_b - Z_a = 1$. At an incident energy of 29 MeV [19], there is about a 35% beneficial increase in the calculated deuteron spectrum at the

lower emission energies. (Triton spectra were not measured.) For comparison, the corresponding data on ^{28}Si [20,21] show about a 20–25% increase. At 49 MeV, the effects are slightly smaller, as shown in Fig. 5. The calculated deuteron intensity from ^{27}Al is increased by about 25%, very slightly improving agreement with experiment [19], whereas the calculated triton cross section is slightly worsened with an increase of roughly 40% at the lower emission energies. Again the ^{28}Si data show similar but smaller changes. At 63 MeV, the effects are significantly smaller.

For (p, xC) reactions, the largest effect is observed in the ^{27}Al$(p, {}^{3}$He$)$ reaction, which was measured at 61.5 MeV [22]. These results are shown in Fig. 6 along with those for two iron targets. Once again, the emitted particle has one more proton than the projectile. A beneficial increase of 30–35% is seen in the lower half of the spectrum. A similar size effect but one that is restricted to a slightly smaller region of the spectrum is seen in the ^{54}Fe$(p, {}^{3}$He$)$ and ^{56}Fe$(p, {}^{3}$He$)$ reactions [22]. The changes result in better agreement with experiment in the spectral shape, whereas the intensity agreement is slightly better for ^{54}Fe and slightly worse for ^{56}Fe. All other changes, including those for ^{27}Al at 90 MeV [23], are much smaller, and many spectra are virtually unchanged.

For complex particle induced reactions, the existing fits must still be regarded as preliminary, because projectile breakup is not yet included in the calculations and may well lead to a change in the exciton model configuration from which the first particle emission is allowed to occur. The latter is here taken to be $(p, h) = (A_a + 1, 1)$, the configurations formed after the first particle-hole pair creation interaction, but could become $(p, h) = (A_a, 0)$ [2]. Nevertheless, the observed effects of the extra residual configurations here are similar to those for nucleon-induced reactions. There is only one $(^{3}$He$, t)$ spectrum in the database—^{62}Ni$(^{3}$He$, t)$ at 24 MeV [24]—and the calculated spectrum is dominated by nucleon transfer at high emission energies and by evaporation at low emission energies, so no noticeable effect is observed from the added residual configurations in the exciton model component. The largest changes in the calculated spectra in this work are in the deuteron-induced pickup channels on ^{27}Al and ^{58}Ni at 80 MeV [25] shown in Fig. 7. The ^{27}Al$(d, {}^{3}$He$)$ and (d, α) reactions show the largest effects—a 40% to 50% increase in intensity at the lower emission energies—with the corresponding ^{58}Ni effects being only slightly smaller. The changes are beneficial for the α spectra but worsen agreement for the ^{3}He spectra. Heavier targets show very little change. For ^{3}He-induced reactions, the largest changes are in the ^{57}Fe$(^{3}$He$, \alpha)$ reaction at 25.6 [26] and 41.4 MeV [27], which

show a 10–15% increase in the lower half of the spectrum. Changes for α-particle-induced reactions are all small because the emitted particles considered all have $A_b \leqslant 4$.

V. SUMMARY AND CONCLUSIONS

The work reported here has solved the problem of the calculated spectral endpoint that was noted in earlier work by including in the residual nucleus state densities those configurations that can physically be populated but that were not being counted. This addition involves no new model parameters. It has, however, necessitated minor adjustments in the relative normalizations of the effective mean square matrix elements for the residual two-body interactions, increasing M_{pp}^2 relative to M_{pn}^2 and M_{nn}^2. Because the previous normalizations were empirical and were chosen to reproduce the observed relative yields in the four (N, N) channels, the need for these adjustments should not be surprising. In addition, the rapidity with which shell effects are assumed to wash out in moving away from a closed-shell configuration was reduced in the preequilibrium calculations.

For (N, N) exchange reactions, agreement in spectral endpoint is consistently and almost universally improved when the added configurations make a significant contribution to the total spectrum. Nucleon inelastic scattering results are virtually unchanged, and the relative intensities in the competing channels are generally unchanged or also improved. For reactions with complex particle channels, direct reaction components obscure the spectral endpoint effects, and the various spectral intensity changes that occur when the added configurations are important, are typically larger, being sometimes beneficial and sometimes detrimental. The situation for reactions with complex particle projectiles will need to be revisited once a projectile breakup model is included in the calculations.

Thus the endpoint problem has been solved without the addition of new model parameters and without changing the overall level of agreement with experiment in other aspects of the calculations, and many of the previously calculated results, especially those on targets above mass 60, are virtually unchanged.

[1] C. Kalbach, J. Phys. G: Nucl. Part. Phys. **24**, 847 (1998).

[2] C. Kalbach, Phys. Rev. C **71**, 034606 (2005).

[3] C. Kalbach, J. Phys. G: Nucl. Part. Phys. **21**, 1519 (1995).

[4] Constance Kalbach Walker, Triangle Universities Nuclear Laboratory Report "Users Manual for PRECO-2000," 2001 (unpublished), available from the code distribution center at the National Nuclear Data Center (Brookhaven National Laboratory) and through the Radiation Safety Information Computing Center (Oak Ridge National Laboratory).

[5] C. Kalbach, Phys. Rev. C **69**, 014605 (2004).

[6] C. Kalbach, Phys. Rev. C **72**, 024607 (2005).

[7] C. Kalbach, Phys. Rev. C **62**, 044608 (2000).

[8] S. M. Grimes, R. C. Haight, and J. D. Anderson, Nucl. Sci. Eng. **62**, 187 (1977).

[9] S. M. Grimes, R. C. Haight, K. R. Alvar, H. H. Barschall, and R. R. Borchers, Phys. Rev. C **19**, 2127 (1979).

[10] G. Traxler, A. Chalupka, R. Fischer, B. Strohmaier, M. Uhl, and H. Vonach, Nucl. Sci. Eng. **90**, 174 (1985).

[11] N. Koori, Y. Ohsawa, and I. Kumabe, Nucl. Sci. Eng. **87**, 34 (1984).

[12] R. Fischer, M. Uhl, and H. Vonach, Phys. Rev. C **37**, 578 (1988).

[13] S. M. Grimes, R. C. Haight, and J. D. Anderson, Phys. Rev. C **17**, 508 (1978).

[14] W. Scobel, M. Blann, T. T. Komoto, M. Trabandt, S. M. Grimes, L. F. Hansen, C. Wong, and B. A. Pohl, Phys. Rev. C **30**, 1480 (1984).

[15] C. Kalbach, Phys. Rev. C **33**, 818 (1986).

[16] A. J. Koning and M. C. Duijvestijn, Nucl. Phys. **A744**, 15 (2004).

[17] R. C. Haight, S. M. Grimes, R. G. Johnson, and H. H. Barschall, Phys. Rev. C **23**, 700 (1981).

[18] W. Scobel, L. F. Hansen, B. A. Pohl, C. Wong, and M. Blann, Z. Phys. A **311**, 323 (1983).

[19] S. Benck, I. Slypen, J. P. Meulders, and V. Corcalciuc, At. Data Nucl. Data Tables **78**, 161 (2001), and data tables supplied by the authors.

[20] F. B. Bateman, R. C. Haight, M. B. Chadwick, S. M. Sterbenz, S. M. Grimes, and H. Vonach, Phys. Rev. C **60**, 064609 (1999), and data tables supplied by the authors.

[21] S. Benck, I. Slypen, J. P. Meulders, and V. Corcalciuc, Nucl. Sci. Eng. **141**, 55 (2002), and data tables supplied by the authors.

[22] F. E. Bertrand and R. W. Peelle, Phys. Rev. C **8**, 1045 (1973).

[23] J. R. Wu, C. C. Chang, and H. D. Holmgren, Phys. Rev. C **19**, 698 (1979).

[24] J. Bisplinghoff, J. Ernst, R. Lohr, T. Mayer-Cuckuk, P. Meyer, Nucl. Phys. **A269**, 147 (1976).

[25] J. R. Wu, C. C. Chang, and H. D. Holmgren, Phys. Rev. C **19**, 370 (1979).

[26] A. Chevarier, N. Chevarier, A. Demeyer, A. Alevra, R. Dumitrescu, I. R. Lukas, M. T. Magda, and M. E. Nistor, Nucl. Phys. **A231**, 64 (1974).

[27] A. Chevarier, N. Chevarier, A. Demeyer, G. Hollinger, P. Pertosa, and Tran Minh Duc, Phys. Rev. C **11**, 886 (1975).